Petroleum Science 20 (2023) 1885–1894

Contents lists available at ScienceDirect

Petroleum Science

journal homepage: www.keaipublishing.com/en/journals/petroleum-science

Original Paper

Effects of the properties of FCCS on the removing of catalyst particles from FCCS under a DC electrostatic field

Qiang Li*, Qing-Zhu Qiu, Hao Cao, Hui-Zhen Yang, Wei-Wei Xu, Zhao-Zeng Liu

College of New Energy, China University of Petroleum (East China), Qingdao, Shandong 266580, China

ARTICLE INFO

Article history:
Received 3 April 2022
Received in revised form
3 September 2022
Accepted 29 November 2022
Available online 30 November 2022

Edited by Jia-Jia Fei

Keywords:
Fluid catalytic cracking slurry (FCCS)
Separation efficiency
Viscosity
Temperature
Four components' mass ratio

ABSTRACT

Catalytic cracking is the main method to lighten heavy crude oil, this process can produce high quality oil products such as gasoline and diesel, but also produces a large amount of fluid catalytic cracking slurry (FCCS). The catalyst particles in FCCS seriously restrict the secondary processing of FCCS and need to be removed, and the properties of FCCS is an important factor that affects the removal efficiency of the catalyst particles. Based on the "effective contact point" model proposed by the research group, this study further proposed the "electrostatic separation efficiency calculation" model. In this model, since FCCS has a uniform distribution of catalyst particles, the ratio of the number of catalyst particles can be expressed as the ratio of area to achieve the calculation of separation efficiency. Then the catalyst removal efficiency under different viscosity was analyzed, thus verifying the feasibility of this model. The effects of temperature and mass ratio of four components on the viscosity of FCCS were investigated respectively, then the effects of temperature and four components' mass ratio on the electrostatic separation can be directly converted into the effect of viscosity on the electrostatic separation efficiency. All the results show the electrostatic separation efficiency decreases with increasing viscosity, and the best separation temperature is 120 °C.

1. Introduction

Catalytic cracking is one of the most important processes for lightning heavy crude oil. The process takes place in a "riser-regenerator" conjugate system, allowing heavy oils to undergo cracking, isomerization, dealkylation and other reactions for the production of lighter oils, olefins, aromatics and other basic chemical raw materials (Ivashkina et al., 2017; Zhou et al., 2021). FCCS (Fluid catalytic cracking slurry) is a by-product in the catalytic cracking process (Zhang et al., 2019). Because of its high content of 2–5 ring short chain aromatics, FCCS can be processed to produce additional products for different applications, such as needle coke, carbon fiber, carbon black, industrial rubber softener, heat transfer oil, etc. (Dong et al., 2005; Eser and Wang, 2007; Lin et al., 2017a; Zhang et al., 2018). Catalyst particles reduce the quality of high value-added products produced from FCCS, so they need to be removed from the FCCS. Sedimentation, filtration, centrifugation and electrostatic separation are the main methods for removing solid particles from FCCS (Fritsche, 1977; Fing et al., 2012; Lin et al., 2017b; Li et al., 2019a). Among them, the electrostatic separation method has a broad application prospect in the FCCS desolidification with its characteristics of small pressure drop, large processing capacity, and suitable for the removal of fine particles (Mazumder et al., 2005). The electrostatic separator for FCCS purification was designed by Gulf Science Technology Company and put into production in 1979 (Fritsche and Stegelman, 1980). Subsequently, various forms of electrostatic separators have emerged, generally containing internal and outer electrodes, with fillers between the two electrodes. When the device operates, the high voltage electric field between the two electrodes will polarize the packing and produce a high electric field intensity gradient near the contact point of the packing, and the catalyst particles will be adsorbed on the surface of the packing due to the positive dielectrophoretic force to purify the slurry.

There was some literature on the electrostatic adsorption process of catalyst particles. Lin and Benguigui (1981) analyzed the effects of different parameters on the solid particles' forces in the non-uniform electric field. Benguigui and Lin (1982) found that the electrostatic separation method is suitable for FCCS, when the FCCS

* Corresponding author.
E-mail address: liqiangsydx@163.com (Q. Li).

https://doi.org/10.1016/j.petsci.2022.11.024

has a low concentration solid phase and the high resistivity liquid phase. Fang et al. discovered the phenomenon of "point adsorption" when they conducted experiments on FCCS purification with a transparent electrostatic separator (Fang et al., 1998). In the author's previous studies (Li et al., 2019a, 2020a, 2020b), the relationship between the angle of the filler contact point and the electric field distribution was fully discussed, then the "effective contact point" model was proposed and verified. Li et al. found the "effective adsorption region" through microscopic experiments and obtained the model to calculate the size of the region through numerical simulation (Li et al., 2020b). In previous research, the electrostatic separation efficiency was expressed in two methods: one method is that the separation efficiency was expressed as the change in catalyst concentration of FCCS before and after electrostatic separation in the experiment; in the other method is that the separation efficiency was expressed by the change in the number of particles adhering to the boundary before and after electrostatic separation in the simulation. There were less models to calculate the electrostatic separation efficiency. Therefore, this study proposed the electrostatic separation efficiency calculation model based on the author's previous models.

The properties of FCCS were influenced by many factors such as the feedstock and the FCC process. Sun et al. found that the separation efficiency of heavy FCCS was lower than that of wax oil FCCS under the same separation conditions when using a standard electrostatic separator (Sun et al., 2016). According to China's heavy oil classification standard, petroleum with viscosity in the range of 100–10000 mPa s at 50 °C will be classified as heavy oil. The viscosity range of FCCS in this experiment is 200–400 mPa s at 50 °C, so the FCCS can also be considered as heavy oil. By regression analysis of the viscosity-temperature curve of heavy oil, Zhao et al. found that the trend is in accordance with the Arrhenius equation, from which it is obvious that the viscosity of heavy oil increases exponentially with increasing temperature (Zhao et al., 2016). Peng and Gu (2007) found that the viscosity of heavy oil increases exponentially with the content of asphaltene but ignored the effect of saturated fraction, aromatic fraction and asphaltene through experimental research. Zhao et al. defined the ratio of the mass of resins and asphaltenes as the colloidal stability coefficient and found that the viscosity of heavy oil decreases as it increases (Zhao et al., 2016).

In summary, the viscosity of FCCS is mainly influenced by two factors: temperature and the mass ratio of the four components. Therefore, this study investigated the effect of temperature and four-component mass ratio on the electrostatic separation efficiency by the experiments and numerical simulation. Firstly, the effect of temperature and four-component mass ratio on the viscosity of FCCS was investigated, then the relationship between separation efficiency and viscosity can be expressed by the electrostatic separation efficiency calculation model. The results of this study can establish an approximate expression for the accurate calculation of separation efficiency, which can be beneficial to obtain the highest value of the electrostatic separator for different FCCS in industry theoretically.

2. Experimental setup and model description

2.1. Experimental setup of electrostatic separation

The electrostatic separation device for this experiment is shown in Fig. 1, and its internal structure is shown in Fig. 2. The device includes a high-voltage DC power supply, a cylindrical electrostatic separator and a temperature control and regulation section. The cylindrical electrostatic separator is made of three layers of stainless steel welded together, the inner layer is the reaction part of the FCCS, the middle layer is filled with thermal conductive oil for heating the FCCS, and the outer layer is filled with insulation material for the insulation of this electrostatic separator. The diameters of the inner layer and inner electrode are 65 mm and 10 mm respectively, and the inner electrode serves as the anode and is connected to a high-voltage DC power supply. The cylinder wall is connected to a ground wire as the cathode. The inner cylinder wall and the center electrode are filled with 4 mm diameter glass bead filler. The temperature control and regulation system consist of a temperature controller, a heating rod and a thermocouple sensor.

In this experiment, the solid content of the FCCS before and after electrostatic separation was measured by the weight method with the following equation.

$$\eta_E = \left(1 - \frac{\omega'}{\omega}\right) \tag{1}$$

In Eq. (1), η_E is the separation efficiency in the experiments, ω' is the solid content of the FCCS after separation, ω is the solid content of the FCCS before separating.

The effect of parameters such as applied voltage, separation time and packing diameter on the electrostatic separation efficiency has been investigated in the authors' previous research (Li et al., 2019a). In this experiment, only the effect of temperature and components of FCCS on the electrostatic separation were studied. So, the voltage of 8 kV DC was applied to the internal electrode, the separation time was 40 min, and the packing diameter was 4 mm.

The auxiliary experimental equipment included electronic balance, constant temperature water tank, constant temperature oil bath, vacuum drying box, motor stirrer and vacuum pump, the device and instrument model are shown in Table 1.

2.2. FCCS property testing devices

In this research, the SARA method was employed to measure four components (saturate, aromatic, resin and asphaltene) mass ratios in the FCCS of the experiments, and the detection devices are shown in Fig. 3. Thermostatic oil baths, evaporative reflux units, and distillation units are shown in Fig. 3a, vacuum drying oven is shown in Fig. 3b, vacuum pump is shown in Fig. 3c, glass adsorption columns and super thermostat baths are shown in Fig. 3d. The specific experimental steps are as follows: The slurry was first refluxed and precipitated with *n*-heptane to separate asphaltenes and soluble matter. After that, the soluble matter was separated from the four components on activated neutral alumina: the chromatographic column was flushed with a 1:1 mixture of *n*-heptane, toluene, ethanol and toluene-ethanol in the order of *n*-heptane, toluene, ethanol and toluene-ethanol, so that each component alternately underwent the adsorption-desorption process in the stationary phase and was continuously exchanged and recombined in the mobile phase to finally achieve the complete separation of the four components.

2.3. Model description

The catalyst particles are subjected to dielectrophoretic force, the effective gravitational force, the Stokes drag force, Brownian and electrostatic interaction forces during the electrostatic

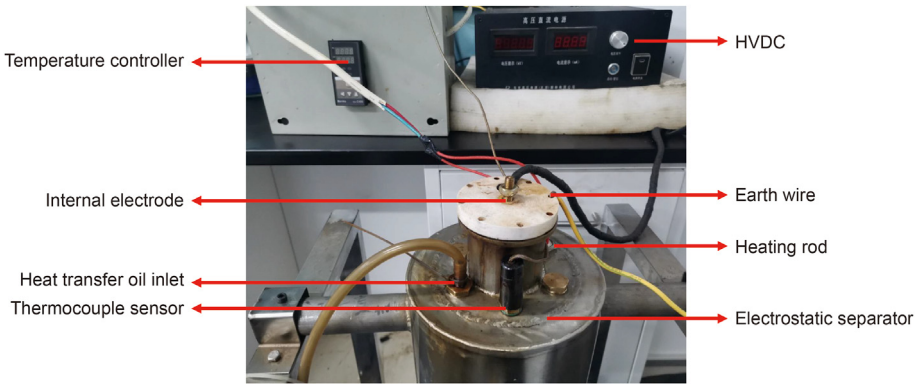

Fig. 1. Schematic diagram of the electrostatic separation device.

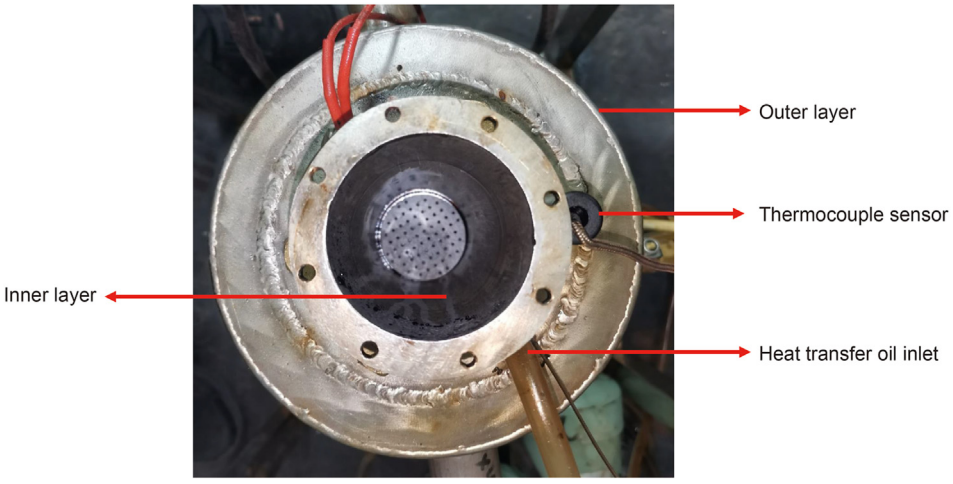

Fig. 2. Internal structure of the electrostatic separator.

Table 1
Auxiliary experimental equipment and instruments.

Devices and equipment	Model
Electronic balance	BSA224S
Motor Stirrer	JJ-1A
Vacuum drying box	DZF-50
Vacuum pump	2ZX-1
Vacuum drying oven	DZF-50
Soxhlet extractor	–
Sand core filter	–

adsorption process. Due to the small size of the catalyst particles, the effect of Brownian motion on the particles is ignored. Because the solid phase concentration of FCCS is low, and the distance between the particles is much larger than the particle size, the effect of electrostatic interaction is ignored. Therefore, the forces on the catalyst particles are shown in Eq. (2).

$$\sum F = F_{DEP} + F_{SD} + F_{EG} \tag{2}$$

In Eq. (2), F_{DEP} is the dielectrophoretic force; F_{SD} is the Stokes drag force; F_{EG} is the effective gravitational force.

The catalyst particles are polarized by the high voltage electrostatic field, then the particles are adsorbed onto the packing surface by the dielectrophoretic force. The dielectrophoretic force plays a driving role in the process of particles adsorption, and it is shown in Eq. (3).

$$F_{DEP} = 2\pi\varepsilon_f r_p^3 \left(\frac{\varepsilon_p - \varepsilon_f}{\varepsilon_p + 2\varepsilon_f}\right) \nabla|E|^2 \tag{3}$$

In Eq. (3), r_p is the particle radius, mm; ε_f and ε_p are the dielectric constant of the oil slurry and the particle respectively, F/m; E is the root-mean-square electric field, V/m.

The catalyst particles are subject to the resistance of the oil slurry during the movement of the electrostatic separation, and this force is called Stokes drag force. The Stokes drag force is shown in Eq. (4).

$$F_{SD} = -\frac{4\pi r_p^3 \rho_p}{3\tau_p}\left(u_p - u_f\right) \tag{4}$$

In Eq. (4), ρ_p is the density of particles, kg/m^3; τ_p is the particle velocity response time, s; u_p and u_f are the velocities of particles and oil slurry, m/s. Because the Reynolds number is low and is in the Stokes zone, $\tau_p = \frac{2\rho_p r_p^2}{9\mu}$. Therefore, the Stokes drag force on the particles can be expressed by Eq. (5).

$$F_{SD} = -6\pi\mu r_p\left(u_p - u_f\right) \tag{5}$$

In Eq. (5), μ is the dynamic viscosity of the FCCS, Pa·s.

Fig. 3. FCCS property testing devices.

The gravitational force on the particles is expressed as Eq. (6).

$$F_G = \frac{4}{3}\rho_p g \pi r_p^3 \tag{6}$$

In Eq. (6), g is the gravitational acceleration, 9.8 m/s^2.

The buoyancy force on the particles is expressed as Eq. (7).

$$F_b = \frac{4}{3}\rho_f g \pi r_p^3 \tag{7}$$

In Eq. (7), ρ_f is the density of oil slurry, kg/m^3. The resultant force of gravity and buoyancy are the effective gravity, which is shown in Eq. (8).

$$F_{EG} = \frac{4}{3}\pi r_p^3 \left(\rho_p - \rho_f\right) g \tag{8}$$

3. The model of electrostatic separation efficiency calculation

Separation efficiency is an important parameter to measure the separation performance of electrostatic separators. The representation of electrostatic separation efficiency in the experimental research is shown in Eq. (1), and the simulation is shown in Eq. (9).

$$\eta_S = \frac{N'}{N} \tag{9}$$

In Eq. (9), η_S is the separation efficiency in the simulation, N is the total number of particles released in the simulation, N' is the number of particles adsorbed to the packing surface.

There was no literature on the theoretical calculation of electrostatic separation efficiency, so this section proposed the electrostatic separation efficiency calculation model based on the authors' "the effective contact point" and "effective adsorption area" model (Li et al., 2019b, 2020b). The "the effective contact point" theory is shown in Eq. (10), which shows that the electric field strength at the contact point is affected by the angle between the line connecting the centers of the two packed spheres and the direction of the applied electric field. When this angle increases gradually, the adsorption capacity for particles at the contact point gradually decreases.

$$E = \frac{3aU\sqrt{\left(\varepsilon_g^2 - \varepsilon_f^2\right)\cos^2\theta + \varepsilon_f^2}}{r(2+\varepsilon_g)\varepsilon_f \ln(R_{out}/R_{in})} \tag{10}$$

where, the correction factor is expressed as a; the angle between the line connecting the centers of the two packed spheres and the direction of the applied electric field is expressed as θ; the radial position of the contact point is expressed as r, mm; the radius of the inner electrodes is expressed as R_{in}, mm; the radius of the outer electrodes is expressed as R_{out}, mm.

Dong et al. concluded that when rigid spheres of equal diameter were poured into a cylindrical container in the natural state, the hexagonal densest pile-up form accounted for more of the pile-up pattern of the spheres (Dong et al., 2009). So, in this section, the effects of viscosity on the separation were investigated in the hexagonal stacking condition. Fig. 4a below shows the stacking state of the filler in a flat state, and Fig. 4b shows the enlarged view of the gap between the fillers, with the three contact points marked as A, B and C. The contact points between the fillers divide the area inside the electrostatic separator into connected tiny adsorption

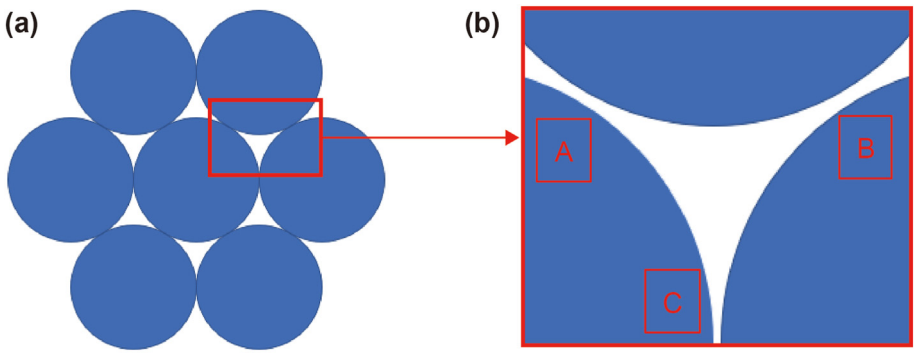

Fig. 4. Schematic diagram of packing plane hexagonal dense accumulation.

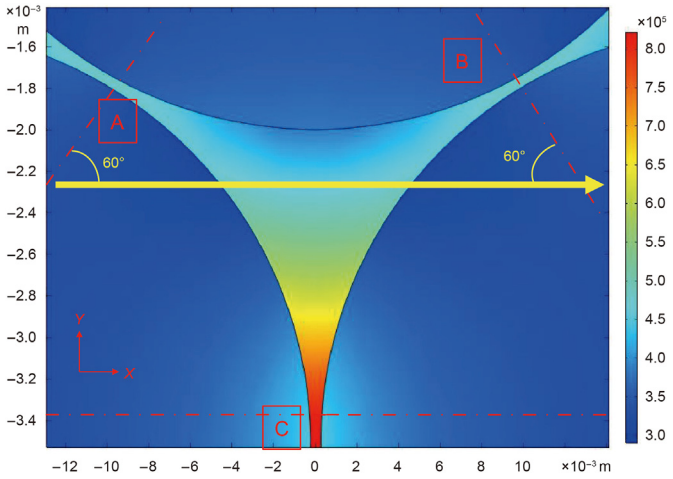

Fig. 5. Electric field strength distribution and isopleth diagram.

areas. The potential difference generated by the original electric field in the direction of the packing diameter can be expressed by Eq. (11).

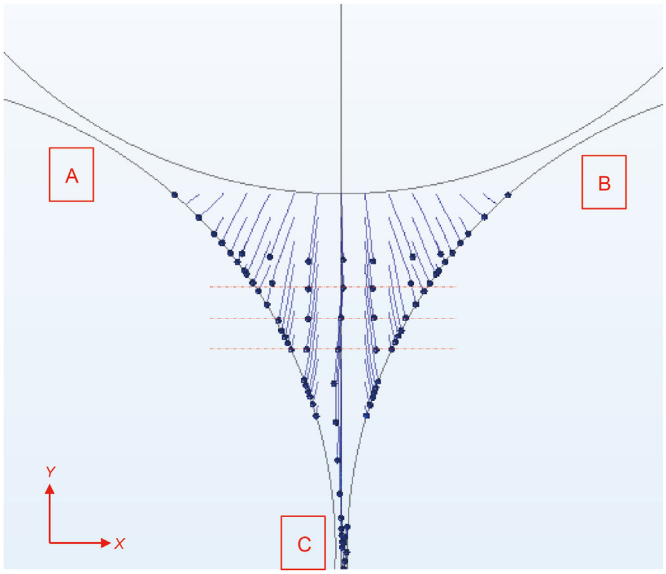

Fig. 6. Particles adsorption motion trajectory.

$$\Delta U = \frac{U_a}{\ln(R_{out}/R_{in})} \times \ln\left(\frac{R_1 + d_g}{R_{in}}\right) - \frac{U_a}{\ln(R_{out}/R_{in})} \times \ln\left(\frac{R_1}{R_{in}}\right) \tag{11}$$

$$= \frac{U_a}{\ln(R_{out}/R_{in})} \times \ln\left(\frac{R_1 + d_g}{R_1}\right)$$

In Eq. (11), ΔU is the potential difference between the two ends of a single packing, R_{in} and R_{out} are the radius of the inner and outer electrodes of the electrostatic separation device respectively, d_g is the diameter of a single packing, R_1 is the shortest distance from the packing surface to the inner electrode. From Eq. (11), it can be found that when d_g is much smaller than R_1, $\frac{R_1+d_g}{R_1} \approx 1$, then $\Delta U \approx 0$, so the electric field generated by the original electric field in the direction of the packing diameter can be approximated as a uniform electric field.

The electric field applied in the separation area of Fig. 5 can be regarded as a uniform electric field, and the direction of the electric field is along the X-axis. At the A and B points, both angles between the direction of the original electric field strength and the line through the filler center are 60°. At the C points, the angle is 0°. Fig. 5 shows that the electric field strength at point C is higher than the electric field strength near it, while the electric field strength at points A and B is closer to the electric field strength near them. When the polarization of the particles is greater than that of the medium, the particles move in the direction of increasing electric field strength, because the relative permittivity of the FCCS is smaller than that of the solid particles, only the C point is the adsorption point of the solid particles. The motion adsorption trajectory of the particle is shown in Fig. 6, the particles move in the direction of the C contact point, which is in accordance with "the effective contact point" theory.

FCCS is a stable colloid, with uniform distribution of catalyst particles and relatively stable solid content. So, the number of catalyst particles is expressed as the product of the area occupied by the particles and the particle surface density, shown in Eq. (12).

$$N = \rho S \tag{12}$$

In Eq. (12), N is the number of particles; ρ is the density of particles per unit area; S is the area occupied by the particles, m^2.

From Fig. 6, the particles are connected along the X-axis direction as shown by the red line during the adsorption motion, and the X-axis direction lines between the particles remain parallel. So, the catalyst particles moving in this region can be regarded as parallel lines, as shown in Fig. 7, the area of the region can be expressed as Eq. (13).

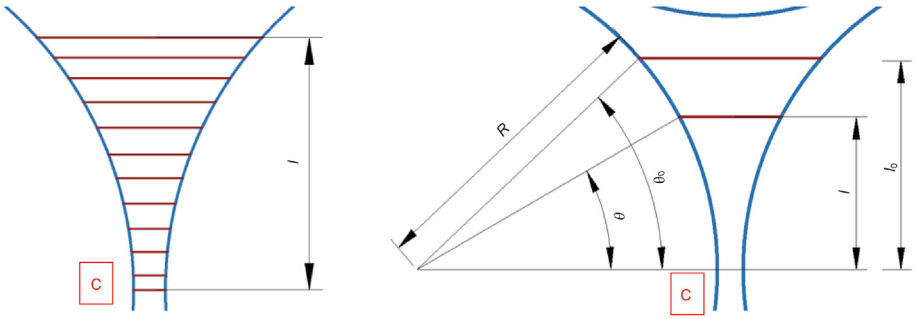

Fig. 7. Differential diagram of adsorption area.

$$S=\int_0^l f(l)\mathrm{d}l \tag{13}$$

In Eq. (13), l is the distance between the particle connection line and the contact point, since $\sin\theta=\frac{l}{R}$, Eq. (13) can be expressed as Eq. (14).

$$S=\left(2R-\sqrt{R^2-l^2}\right)l-R^2\arcsin\frac{l}{R} \tag{14}$$

According to the "effective adsorption area" theory, maximum adsorption distance l_0 exists between particles and contact points, which is shown in Eq. (15).

$$l_0=8.26\times U^{-0.014}\times q^{-0.026}-12.5 \tag{15}$$

In Eq. (15), U is the applied voltage, V; q is charge density, C/m^3.

When the particles located at a distance l_0 from the contact point C move to the position l away from the contact point C, the reduction of the area occupied by the particles is shown in Eq. (16). The number of particles adsorbed on the packing surface is shown in Eq. (17). Therefore, the separation efficiency can be expressed by Eq. (18).

$$\begin{aligned}\Delta S=S_0-S=&\left(2R-\sqrt{R^2-{l_0}^2}\right)l_0-R^2\arcsin\frac{l_0}{R}\\&-\left(2R-\sqrt{R^2-l^2}\right)l+R^2\arcsin\frac{l}{R}\end{aligned} \tag{16}$$

$$N'=\rho\Delta S \tag{17}$$

$$\eta=\frac{N'}{N}=\frac{\rho\Delta S}{\rho S_0}=\frac{S_0-S}{S_0}=1-\frac{S}{S_0} \tag{18}$$

The velocity of particles in motion from l_0 to l can be expressed by Eq. (19).

$$u=\frac{\mathrm{d}(l_0-l)}{\mathrm{d}t} \tag{19}$$

In the two-dimensional interface, the particles are only subject to the action of the dielectrophoretic force and the drag force. Therefore, the momentum equation of catalyst particles can be expressed as Eq. (20).

$$\frac{\pi}{4}d_\mathrm{p}^3\frac{\varepsilon_\mathrm{f}\left(\varepsilon_\mathrm{p}-\varepsilon_\mathrm{f}\right)}{\varepsilon_\mathrm{p}+2\varepsilon_\mathrm{f}}\nabla|E|^2-\frac{1}{\tau_\mathrm{p}}m_\mathrm{p}u_\mathrm{n}=m_\mathrm{p}\frac{\mathrm{d}u_\mathrm{n}}{\mathrm{d}t} \tag{20}$$

The slurry was stationary during the electrostatic separation process, so $v=0$. And the solution of Eq. (20) is shown in Eq. (21).

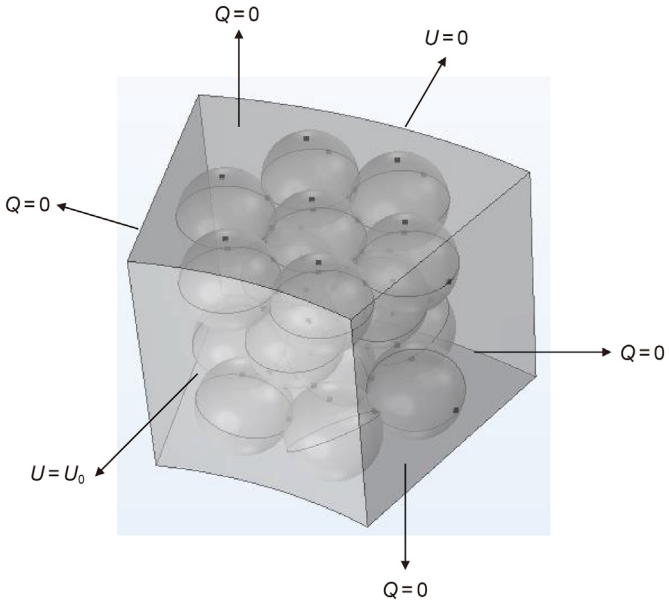

Fig. 8. Schematic diagram of geometric model and boundary conditions.

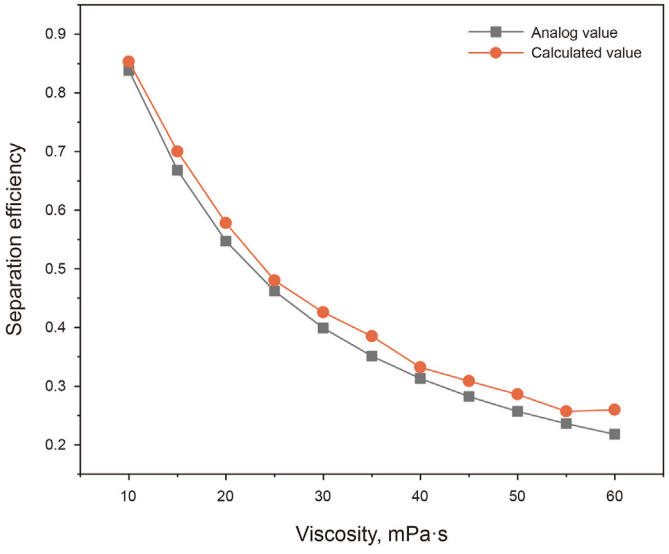

Fig. 9. The variation of separation efficiency with the viscosity.

$$u=\frac{\varepsilon_f\left(\varepsilon_p-\varepsilon_f\right)d_p^2}{12\mu\left(\varepsilon_p+2\varepsilon_f\right)}\cdot\nabla|E|^2\left(1-e^{\frac{-18\mu}{d_p^2\rho_f}t}\right) \tag{21}$$

From Eq. (21), when $t>10^{-6}$ s, $e^{\frac{-18\mu}{d_p^2\rho_f}t}\approx 0$. When $t=0$ s, the particles have no motion displacement, then the motion displacement of the particles can be expressed by Eq. (22).

$$l_0-l=\int u\mathrm{d}t=\frac{\varepsilon_f\left(\varepsilon_p-\varepsilon_f\right)d_p^2t}{12\mu\left(\varepsilon_p+2\varepsilon_f\right)}\cdot\nabla|E|^2 \tag{22}$$

Finally, the model of electrostatic separation efficiency calculation can be expressed by Eq. (23).

$$\begin{aligned}\eta&=1-\frac{\left(2R-\sqrt{R^2-l^2}\right)l-R^2\arcsin\frac{l}{R}}{\left(2R-\sqrt{R^2-l_0^2}\right)l_0-R^2\arcsin\frac{l_0}{R}}\\ l_0-l&=\frac{\varepsilon_f\left(\varepsilon_p-\varepsilon_f\right)d_p^2t}{12\mu\left(\varepsilon_p+2\varepsilon_f\right)}\cdot\nabla|E|^2\\ l_0&=8.26\times U^{-0.014}\times q^{-0.026}-12.5\end{aligned} \tag{23}$$

To verify the accuracy of the electrostatic separation efficiency calculation model, the simulation model was built as shown in Fig. 8. The front side of the geometric model serves as an anode and is connected to the power supply, the voltage is expressed as U_0; the back side of the geometric model serves as the cathode and its voltage is 0 V the remaining surfaces are insulated.

In this study, the applied voltage is 8 kV and the charge density is 4e−11 C/m^3, from Eq. (15), l_0 is 1.07 mm. The applied voltage is the same in the simulation and the electrostatic separation experiment, and adsorption behavior of solid particles is simulated by the fluid flow particle tracking module. The particles were released by using the random release. The electrostatic separation efficiency in the numerical simulation and calculated by Eq. (23) with the velocity changes as shown in Fig. 9, the trend of both is basically consistent and shows a decreasing trend. The maximum value of relative error is 16.1%. Thus, the accuracy of electrostatic separation efficiency calculation model can be verified.

4. Result and analysis

In the previous section, the electrostatic separation efficiency calculation model was proposed and simulated for FCCS of different viscosity. In this section, the effect of the temperature and the four components' mass ratio on electrostatic separation efficiency was divided into two parts: the first part is the effect of the temperature and the four components' mass ratio on the viscosity, the second part is the effect of viscosity on the electrostatic separation efficiency.

4.1. Effect of the temperature on electrostatic separation efficiency

The viscosity of FCCS is high at normal temperature, which has a great adverse effect on the removal of solid particles. The viscosity of FCCS is usually reduced by heating FCCS or adding viscosity-reducing agents. Therefore, this section investigates the effect of the temperature of FCCS on the electrostatic separation efficiency. The mass ratio of saturated, aromatic, resin fraction and asphaltene fraction of the FCCS used in this section is 23.48:64.91:9.28:2.33. In the experiment, the heat transfer oil' temperature in the middle layer of the electrostatic separator is controlled by an automatic temperature control device. As shown in Fig. 10, the variation of viscosity with temperature is shown schematically, the viscosity of catalytic slurry decreases exponentially with temperature.

FCCS is a heavy oil system, and the relationship between viscosity and temperature of heavy oil has been studied by scholars. Zhu et al. obtained exponential viscosity-temperature curves by experimentally fitting multiple groups of heavy oil viscosities from different fields, and these curves all satisfy the form of the Arrhenius equation, which is shown in Eq. (24).

$$\mu=Ae^{E_a/RT} \tag{24}$$

In Eq. (24), T is the thermodynamic temperature, K; A is a constant; R is the universal gas constant (J/K mol); E_a is the activation energy, J/mol; and μ is the viscosity of the heavy oil at the absolute temperature T. Peng and Gu (2007) carried out the experiment of the viscosity and activation energy E_a of heavy oil containing different volume fractions of asphaltene, then Peng Luo concluded

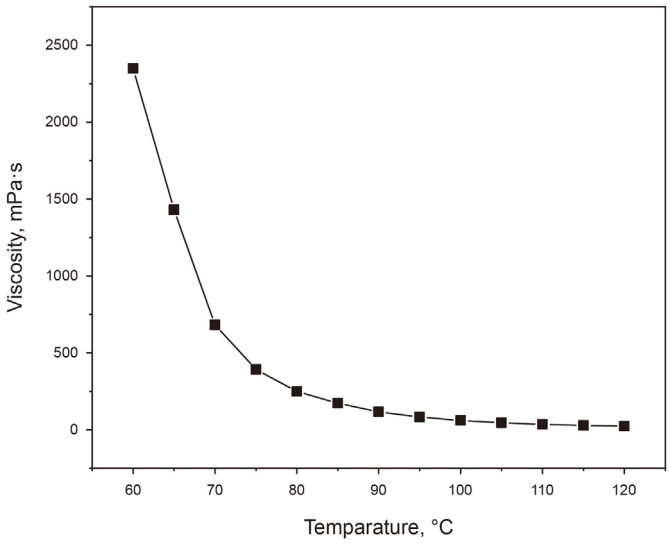

Fig. 10. The variation of viscosity with temperature.

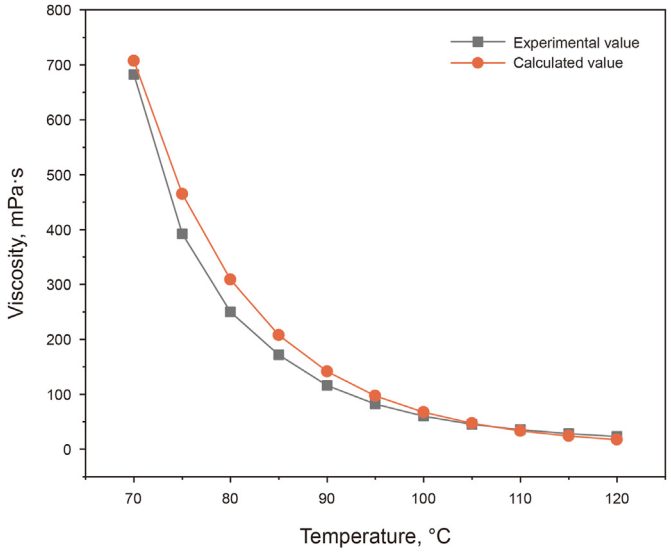

Fig. 11. The variation of viscosity with temperature.

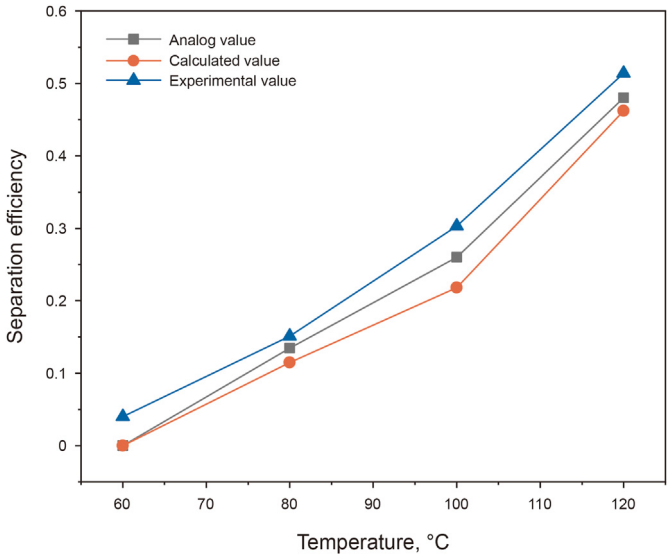

Fig. 12. The variation of electrostatic separation efficiency with temperature.

that the activation energy E_a of heavy oil increases essentially linearly with the volume fraction of asphaltene. Therefore, the percentage of asphaltene does not change abruptly when the FCCS type is constant, and the activation energy E_a is also constant. Eq. (24) can be transformed into Eq. (25).

$$\ln \mu = \frac{E_a}{R} \cdot \frac{1}{T} + \ln a \tag{25}$$

From Eq. (25), the relationship between $\ln \mu$ and $\frac{1}{T}$ varies linearly, and a linear fit yields: $\frac{E_a}{R} = 10032$, $\ln a = -22.674$, and the squared difference $R^2 = 0.9815$. Fig. 11 shows the comparison between the experimental values of the measured viscosity-temperature curves and the calculated values calculated by Eq. (25). Eq. (25) can basically represent the change of the viscosity of the FCCS with the increase in temperature, and the calculated value is closer to the actual viscosity as the temperature increases. Therefore, the effect of temperature on the electrostatic separation efficiency can be directly converted into the effect of viscosity on the electrostatic separation efficiency.

The applied voltage and separation time in the simulation are uniformly consistent with the experimental conditions, and since there is a clear correspondence between the temperature and the viscosity of the FCCS, the viscosity of the FCCS is directly controlled in the simulation to realize the effect of temperature on the electrostatic separation efficiency. As shown in Fig. 12, the electrostatic separation efficiency in the experiment, simulation and calculation gradually increases with the increase of temperature; the change trend of them remains basically the same. Because of gravity in the experiment, the particles undergo a settling behavior, so the results of separation efficiency obtained from simulation and experiment for different temperature cannot be completely consistent. The relationship between the viscosity of FCCS and temperature is shown in Eq. (25), viscosity decreases exponentially with temperature. And according to electrostatic separation efficiency calculation model in Eq. (23), the separation efficiency decreases with increasing viscosity. And the result further proves the feasibility and accuracy of the electrostatic separation efficiency calculation model.

Table 2
Mass fraction of four components of catalytic oil slurry with different viscosities.

Viscosity, mPa·s	w_s, %	w_a, %	w_r, %	w_{as}, %	w_r/w_{as}
12165	19.32	33.54	25.64	21.50	1.19
17331	23.44	29.38	23.11	24.07	0.96
18797	23.98	29.05	23.80	23.17	1.03
22773	25.24	30.01	21.10	23.65	0.89
22936	23.17	29.55	23.69	23.58	1.00
23148	21.78	33.05	22.85	22.32	1.02
23971	22.97	31.59	22.87	22.57	1.01

4.2. Effect of the four components' mass ratio on electrostatic separation efficiency

After studying the effect of temperature on the electrostatic separation of FCCS, the effect of the components of FCCS on the electrostatic separation is investigated. FCCS is an extremely complex mixture of components and can generally be divided into saturated, aromatic, resin and asphaltene. The FCCS is a dispersed system with asphaltene as the core, where saturated, aromatic and resin are used as dispersed phases.

The viscosity of heavy oil increases exponentially with the increase of asphaltene component and decreases exponentially with the increase of saturated and aromatic, and the contribution of asphaltene, saturated fraction and aromatic fraction to the viscosity of heavy oil is 0.95:0.42:0.48 after fitting a large amount of data (Wang et al., 2010). The contribution of asphaltenes to the viscosity of heavy oil is positive, the saturated and aromatic fractions are negative to the viscosity of heavy oil. Resin plays an important role in the stability of colloids, and the increase of gum content decreases the viscosity of FCCS. Therefore, the viscosity of different FCCS can be expressed as Eq. (26).

$$\mu = a \exp\left[b_1(0.51w_{as} - 0.23w_s - 0.26w_a) - b_2\frac{w_r}{w_{as}}\right] \tag{26}$$

w_{as} is the mass fraction of asphaltene, w_s is the mass fraction of saturated fraction, w_a is the mass fraction of aromatic fraction, w_r is the mass fraction of resin fraction, and $\frac{w_r}{w_{as}}$ is the colloidal stability. The parameters a, b_1 and b_2 are constants. The ratio of different FCCS's viscosities related to the components is established by Eq. (27).

$$b = \frac{\mu}{\mu_0} = \exp\left[b_1\Delta(0.51w_{as} - 0.23w_s - 0.26w_a) - b_2\Delta\frac{w_r}{w_{as}}\right] \tag{27}$$

In Eq. (27), b is the ratio of the viscosity of different FCCS.

Table 2 shows the four-component mass fractions and colloidal stability parameters of catalytic slurries with different viscosities measured during the experiment of the research.

The regression analysis was used to derive: $b_1 = 0.0359$, $b_2 = -0.8728$, the constant is 0.0867, regression coefficient $R^2 = 0.8873$, and finally the ratio of viscosity of different FCCS is shown in Eq. (28).

Table 3
Mass fraction of four components of FCCS with different plants.

	w_s, %	w_a, %	w_r, %	w_{as}, %	Viscosity, mPa·s
A	30.7	62.61	1.43	5.26	13.2
B	4.99	82.69	5.87	3.5	52
C	19	75.3	4.42	2.28	57.8
D	26.39	63.88	7.47	2.25	218

Table 4
The relative errors of the viscosity ratios *b* of the four slurries.

b	Actual value	Predicted values	Relative errors
B/A	3.94	3.69	6.31%
C/A	4.38	4.33	1.17%
D/A	16.52	15.11	8.48%

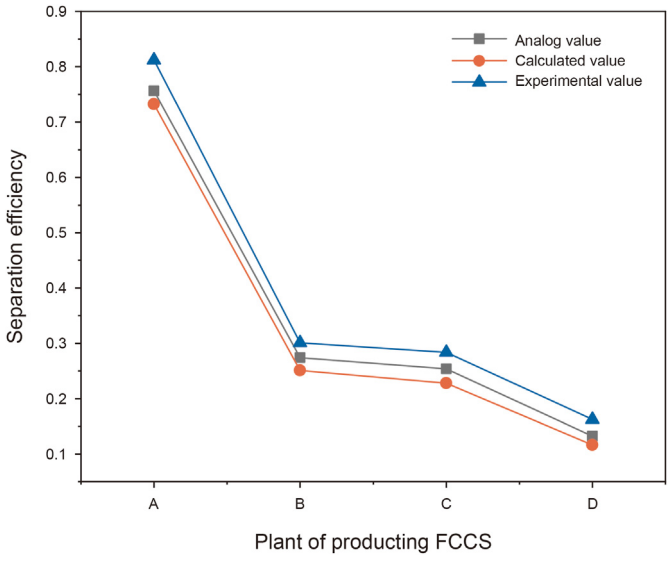

Fig. 13. The variation of electrostatic separation efficiency with different FCCS.

$$b=\frac{\mu}{\mu_0}=\exp\left[0.0359\Delta(0.51w_{as}-0.23w_s-0.26w_a)+0.8728\Delta\frac{w_r}{w_{as}}+0.0867\right] \quad (28)$$

The mass ratio of the four components of the four FCCS (A, B, C and D represent the four catalytic cracking oil slurry plants respectively) was analyzed using the property analysis instrument of FCCS, the results are shown in Table 3. The relative errors of the viscosity ratio *b* of the four slurries are shown in Table 4, and the maximum value of relative error is 8.48%. So, Eq. (28) can basically represent the effect of the components of FCCS on the viscosity of FCCS. Therefore, the effect of four components on the electrostatic separation efficiency can be directly converted into the effect of viscosity on the electrostatic separation efficiency.

Fig. 13 illustrates the influence of the four components' mass ratio on the electrostatic separation efficiency at a separation temperature of 80 °C, and the raw material for the FCCS comes from four plants A, B, C and D, respectively. Because of the complex composition of catalytic slurry, its viscosity is not entirely determined by the mass ratio of the four components. The results of particle adsorption rates obtained from simulation and experiment for different FCCS cannot be completely consistent, but the changing trend of experimental value, analog value and calculated value are the same. The result shows that the qualitative comparison of the electrostatic separation efficiency of different FCCS can be achieved by combining electrostatic separation efficiency calculation model and Eq. (28).

According to the analysis in this paper, the following measures can be taken to improve the separation efficiency.

(1) Adding a viscosity reducer or ultrasonic treatment before electrostatic separation operation to reduce the viscosity of FCCS.
(2) Use packing with larger dielectric constant to increase the squared gradient of electric field strength near the contact point of the packing. In addition, the diameter of the packing should be smaller to increase the number of packing contact points per unit volume in the electrostatic separator.
(3) Appropriately increase the value of the power supply voltage.

5. Conclusion

In this study, the influence of the properties of FCCS on the adsorption of catalyst particles was studied by numerical simulations and experimental investigation. Based on the "effective contact point" and "effective adsorption regions" proposed by our research group, this study proposed the "electrostatic separation efficiency calculation" model. This model is shown as

$$\begin{cases}\eta=1-\dfrac{(2R-\sqrt{R^2-l^2})l-R^2\arcsin\dfrac{l}{R}}{(2R-\sqrt{R^2-l_0^2})l_0-R^2\arcsin\dfrac{l_0}{R}}\\ l_0-l=\dfrac{\varepsilon_f(\varepsilon_p-\varepsilon_f)d_p^2t}{12\mu(\varepsilon_p+2\varepsilon_f)}\cdot\nabla|E|^2\\ l_0=8.26\times U^{-0.014}\times q^{-0.026}-12.5\end{cases}.$$

The catalyst removal efficiency under different viscosity was analyzed, thus verifying the feasibility of this model. This model achieved the calculation of separation efficiency by transforming the ratio of the number of catalyst particles to the ratio of area. In order to put the model into practical production, parameters such as viscosity of FCCS, dielectric constant, the ratio of four component masses and particle size and dielectric constant of catalyst particles need to be determined. The viscosity-temperature curve was derived by fitting the experimental data, the viscosity decreases exponentially with temperature. Then the relationship between temperature and separation efficiency can be obtained by combining the "electrostatic separation efficiency calculation" model and viscosity-temperature curve. After further reference to several sets of data on the four components' mass ratio of heavy oil, the parameter *b* which indicates the viscosity ratio of different FCCS was fitted. Therefore, the effects of the four components' mass ratio on the electrostatic separation can be directly converted into the effect of viscosity on the electrostatic separation efficiency. The results of this study showed the electrostatic separation efficiency decreases with increasing viscosity and the best separation temperature is 120 °C.

Acknowledgements

This work was supported by the [Natural Science Foundation Project of Shandong Province #1] under Grant [ZR2019MEE033]; [Fundamental Research Funds for the central Universities #2] under Grant [19CX02035A].

References

Benguigui, L., Lin, I.J., 1982. Dielectrophoretic filtration of nonconductive liquids. Separ. Sci. Technol. 17 (8), 1003–1017. https://doi.org/10.1080/01496398208060265.
Dong, P., Wang, C., Zhao, S., 2005. Preparation of high performance electrorheological fluids with coke-like particles from FCC slurry conversion. Fuel 84 (6), 685–689. https://doi.org/10.1016/s0140-6701(05)82909-1.
Dong, K.J., Yang, R.Y., Zou, R.P., An, X.Z., Yu, A.B., 2009. Critical states and phase

diagram in the packing of uniform spheres. EPL 86 (4), 46003. https://doi.org/10.1209/0295-5075/86/46003.
Eser, S., Wang, G.A., 2007. Laboratory study of a pretreatment approach to accommodate high-sulfur FCC decant oils as feedstocks for commercial needle coke. Energy Fuel. 21 (6), 3573–3582. https://doi.org/10.1021/ef060541v.
Fang, Y.J., Xiao, W.D., Wang, G.R., 1998. Study on electrostatic separation of solid-liquid systems II. Measurement of saturated adsorption weigh. Petrochem. Technol. 27 (11), 35–39 (in Chinese).
Fing, D., Liu, L., Wang, P., Zhang, H., Xie, X., 2012. The experimental study of natural sedimentation in heavy oil. Mater. Sci. Eng. 413, 60–64. https://doi.org/10.4028/www.scientific.net/AMR.413.60.
Fritsche, G.R., 1977. Electrostatic separator removes FCC catalyst fines from decanted oil. Oil Gas J. 75 (13), 73–81.
Fritsche, G.R., Stegelman, A.F., 1980. Electrostatic catalyst separator upgrades fcc bottoms. Oil Gas J. 78 (40), 55–59.
Ivashkina, E., Nazarova, G., Shafran, T., Stebeneva, V., 2017. Forecasting the zeolite-containing catalyst activity in catalytic cracking technology taking into account the feedstock composition. Oil Gas Eng. 1876, 1–9. https://doi.org/10.1063/1.4998834.
Li, Q., Wu, Z.J., Zhang, Z., Wang, Z.B., Guo, L.F., Li, A.M., 2019a. Experimental study on the removal of FCCS catalyst particles by electrostatic separation. Energy Sources 9, 1–13. https://doi.org/10.1016/b978-0-08-036448-3.50052-9.
Li, Q., Zhang, Z., Wu, Z.J., Wang, Z.B., Guo, L.F., 2019b. Effects of electrostatic field and operating parameters on removing catalytic particles from FCCS. Powder Technol. 342, 817–828. https://doi.org/10.1016/j.powtec.2018.10.060.
Li, Q., Li, A.M., Guo, L.F., Cao, H., Xu, W.W., Wang, Z.B., 2020a. Microscopic mechanistic study on the removal of catalyst particles in FCCS by an electrostatic field. Powder Technol. 363, 500–508. https://doi.org/10.1016/j.powtec.2020.01.019.
Li, Q., Guo, L.F., Cao, H., Li, A.M., Xu, W.W., Wang, Z.B., 2020b. Effects of an effective adsorption region on removing catalyst particles from an FCC slurry under a DC electrostatic field. Powder Technol. 377, 676–683. https://doi.org/10.1016/j.powtec.2020.09.038.
Lin, I.J., Benguigui, L., 1981. Dielectrophoretic filtration and separation: general outlook. Separ. Purif. Methods 10 (1), 53–72. https://doi.org/10.1080/03602548108066007.
Lin, Y., Nan, G.Z., Li, Y.F., Luo, H., Fan, W.Y., 2017a. Ionic-liquid-catalyzed alkylation of extracted oil from a fluid catalytic cracking slurry. Energy Fuel. 31 (11), 11911–11917. https://doi.org/10.1021/acs.energyfuels.7b02227.
Lin, C.H., Wang, J.Q., Wang, Z.X., Liu, H., Chen, K., Guo, A.J., 2017b. Flocculation of particulates in fluid catalytic cracking slurry oil: characterization of the particulates and the effect of thermal treatment on their flocculation. Energy Fuel. 31 (12), 13282–13290. https://doi.org/10.1021/acs.energyfuels.7b02219.
Mazumder, M.K., Sims, R.A., Biris, A.S., Srirama, P.K., Saini, D., Yurteri, C.U., Trigwell, S., De, S., Sharma, R., 2005. Twenty-first century research needs in electrostatic processes applied to industry and medicine. Chem. Eng. Sci. 61 (7), 2192–2211. https://doi.org/10.1016/j.ces.2005.05.002.
Peng, L., Gu, Y., 2007. Effects of asphaltene content on the heavy oil viscosity at different temperatures. Fuel 86 (7–8), 1069–1078. https://doi.org/10.1016/j.fuel.2006.10.017.
Sun, X.W., Chen, Y.L., Zhang, L.Z., Xu, Z.M., Sun, X.W., Zhao, S.Q., Xu, C.M., 2016. Supercritical fluid extraction of fluid catalytic cracking slurry oil: bulk property and molecular composition of narrow fractions. Energy Fuel. 30 (12), 10064–10071. https://doi.org/10.1021/acs.energyfuels.6b01132.
Wang, S.Q., Shen, B., Lin, R.Z., 2010. Correlation for the viscosity of heavy oil and its chemical composition. Acta Petrolei Sinica 26 (5), 795–799 (in Chinese).
Zhang, D.K., Zhang, L.Z., Yu, Y., Zhang, L., Xu, Z.M., Sun, X.W., Zhao, S.Q., 2018. Mesocarbon microbead production from fluid catalytic cracking slurry oil: improving performance through supercritical fluid extraction. Energy Fuel. 32 (12), 12477–12485. https://doi.org/10.1021/acs.energyfuels.8b03498.
Zhang, Z., Li, Q., Wang, Z.Z., Wu, Z.J., Li, A.M., Guo, L.F., 2019. Effect of structural parameters of an electrostatic separator on the removal of catalyst particles from fluid catalytic cracking slurry. Separ. Purif. Technol. 222, 11–21. https://doi.org/10.1016/j.seppur.2019.04.012.
Zhao, R.Y., Zhan, X.C., Zhang, C., Li, C., Yang, C.H., Zhao, Y.S., Zhao, Y.S., 2016. Viscosity influence factors of super heavy crude oil. Oilfield Chem. 33 (2), 319–324 (in Chinese).
Zhou, X., Sun, Z., Yan, H., Feng, X., Yang, C., 2021. Produce petrochemicals directly from crude oil catalytic cracking, a techno-economic analysis and life cycle society-environment assessment. J. Clean. Prod. 308, 1–14. https://doi.org/10.1016/j.jclepro.2021.127283.